On the Susceptibility of Cold Tropical Cirrus to Ice Nuclei Abundance

ERIC J. JENSEN, REI UEYAMA, LEONHARD PFISTER, AND THAOPAUL V. BUI

NASA Ames Research Center, Moffett Field, California

R. PAUL LAWSON AND SARAH WOODS

Spec Inc., Boulder, Colorado

TROY THORNBERRY AND ANDREW W. ROLLINS

NOAA/Earth System Research Laboratory, and Cooperative Institute for Research in Environmental Sciences, Boulder, Colorado

GLENN S. DISKIN, JOSHUA P. DIGANGI, AND MELODY A. AVERY

NASA Langley Research Center, Hampton, Virginia

(Manuscript received 9 September 2015, in final form 25 March 2016)

ABSTRACT

Numerical simulations of cirrus formation in the tropical tropopause layer (TTL) during boreal wintertime are used to evaluate the impact of heterogeneous ice nuclei (IN) abundance on cold cloud microphysical properties and occurrence frequencies. The cirrus model includes homogeneous and heterogeneous ice nucleation, deposition growth/sublimation, and sedimentation. Reanalysis temperature and wind fields with high-frequency waves superimposed are used to force the simulations. The model results are constrained by comparison with in situ and satellite observations of TTL cirrus and relative humidity. Temperature variability driven by high-frequency waves has a dominant influence on TTL cirrus microphysical properties and occurrence frequencies, and inclusion of these waves is required to produce agreement between the simulated and observed abundance of TTL cirrus. With homogeneous freezing only and small-scale gravity waves included in the temperature curtains, the model produces excessive ice concentrations compared with in situ observations. Inclusion of relatively numerous heterogeneous ice nuclei ($N_{IN} \geq 100\,L^{-1}$) in the simulations improves the agreement with observed ice concentrations. However, when IN contribute significantly to TTL cirrus ice nucleation, the occurrence frequency of large supersaturations with respect to ice is less than indicated by in situ measurements. The model results suggest that the sensitivity of TTL cirrus extinction and ice water content statistics to heterogeneous ice nuclei abundance is relatively weak. The simulated occurrence frequencies of TTL cirrus are quite insensitive to ice nuclei abundance, both in terms of cloud frequency height distribution and regional distribution throughout the tropics.

1. Introduction

The formation of ice crystals in the cold upper troposphere has been the subject of numerous investigations over many years, driven in part by the challenges of the problem and in part by the climatic importance of cirrus clouds. These investigations have included laboratory studies of ice nucleation [see Hoose and Möhler (2012) and references therein], field measurements of individual aerosol ice nucleation activity and ice crystal properties (DeMott et al. 2003; Froyd et al. 2010; Cziczo et al. 2013), numerical simulations of ice nucleation (e.g., Kärcher et al. 2006; Spichtinger and Cziczo 2010), and global cirrus simulations using parameterizations of ice nucleation processes (e.g., Lohmann et al. 2004; Gettelman et al. 2015). Here, we use ensembles of detailed cirrus simulations (constrained by cirrus observations) to investigate the implications of different assumptions about ice nucleation processes on the statistical properties of cirrus in the cold, uppermost tropical troposphere.

Corresponding author address: Eric Jensen, NASA Ames Research Center, MS 245-5, Moffett Field, CA 94035.
E-mail: eric.j.jensen@nasa.gov

DOI: 10.1175/JAS-D-15-0274.1

We focus on cirrus forming in the tropical tropopause layer (TTL; between about 15 and 18 km in the tropics). Interest in TTL processes has been motivated by the fact that this layer is generally slowly rising (in balance with radiative heating), and therefore the composition of the TTL represents a lower boundary condition for the stratospheric composition [see Fueglistaler et al. (2009) and references therein]. In particular, growth and sedimentation of cirrus ice crystals in the extremely cold TTL are responsible for dehydration of the air entering the stratosphere to very low water vapor mixing ratios. TTL cirrus are also of interest because of their high occurrence frequency (Wang et al. 1996); the regional TTL cirrus coverage can exceed 50% (Haladay and Stephens 2009; Yang et al. 2010). Even though TTL cirrus are optically thin, the high cloud cover implies a climatically significant radiative forcing (Haladay and Stephens 2009). Also, TTL cirrus radiative heating is a large term in the local thermal budget (Yang et al. 2010), with corresponding effects on the regional temperature and dynamical structure.

At temperatures below about −38°C where existence of pure liquid water is not possible, the potential ice nucleation mechanisms include spontaneous (homogeneous) freezing of aqueous solution drops and heterogeneous nucleation of ice on the surfaces of dry aerosol particles or insoluble inclusions in aqueous aerosols. The key differences between these mechanisms that will affect cirrus occurrence and physical properties are 1) homogeneous freezing of aqueous aerosols requires large supersaturations with respect to ice [≃165% relative humidity with respect to ice (RHI) at TTL temperatures], whereas heterogeneous nucleation can occur at lower supersaturations; and 2) effective heterogeneous nuclei comprise a small subset of the total aerosol population, whereas an abundant supply of aqueous aerosols is always present in the upper troposphere. Therefore, the presence of heterogeneous ice nuclei (IN) can alter the meteorological conditions required for cirrus formation and the microphysical properties (e.g., sizes and concentrations of ice crystals) of the cirrus clouds that form.

Mineral dust and metallic particles have been shown to be particularly effective ice nuclei promoting ice formation in the upper troposphere (DeMott et al. 2003; Cziczo et al. 2013). Both Murray (2008) and Zobrist et al. (2008) proposed that homogeneous nucleation could be delayed or prevented in highly viscous oxidized organic aerosols that are particularly prone to be in semisolid or glassy states at low temperatures prevalent in the TTL. Further work showed that glassy aerosols can act as heterogeneous ice nuclei at low temperatures (Murray et al. 2010; Wilson et al. 2012). However, the detailed chemical composition of organic-containing aerosols in the upper troposphere (and their corresponding effectiveness as heterogeneous ice nuclei) is not known.

Since the atmospheric abundance of mineral dust, metallic, and organic particles is changing in response to human activities, there is potential for anthropogenic modification of cirrus cloud properties, which could in turn alter the Earth–atmosphere radiation budget, the upper-tropospheric heat budget, atmospheric dynamics, stratospheric humidity, and climate. This study addresses the basic questions of whether TTL cirrus ice concentration, extinction, ice mass, and occurrence frequency change significantly in response to changes in heterogeneous ice nuclei abundance.

Cziczo et al. (2013) combined ice crystal residual measurements from a number of airborne field experiments and noted that heterogeneous nucleation appears to play a major role in formation of much of the cirrus sampled (mostly in the midlatitude upper troposphere). However, the relative importance of heterogeneous nucleation in the TTL is not well known. Direct airborne ice nuclei measurements are unavailable at altitudes or temperatures even approaching TTL conditions. High-altitude aircraft measurements of ice crystal residual composition made in the TTL do not indicate a clear enhancement in abundance of known heterogeneous nuclei (such as mineral dust) relative to the ambient aerosol population (Froyd et al. 2010). Nearly every ice crystal residual particle was an internal mixture of neutralized sulfate and organic carbon, with similar compositions to the ambient aerosols. These measurements could be interpreted as lack of evidence for heterogeneous nucleation on a preferred subset of the aerosol population. Alternatively, mixed-organic aerosols in a glassy state may have been acting as heterogeneous nuclei, resulting in ice crystal residuals with similar compositions to the predominantly mixed-organic ambient aerosols. Past studies have hypothesized effloresced ammonium sulfate as another candidate for effective ice nuclei at low temperatures (Abbatt et al. 2006), and enhancement of ammonium sulfate in ice crystal residuals would not necessarily be apparent in particle analysis by laser mass spectrometry (PALMS) measurements. In summary, neither the abundance of effective heterogeneous ice nuclei in the TTL nor the composition of TTL ice nuclei is currently known. Further, the relative importance of heterogeneous and homogeneous nucleation for producing TTL ice crystals is not known.

We assess the representation of cirrus microphysical processes in our numerical simulations by statistically comparing results with recent observations of TTL cirrus from the Airborne Tropical Tropopause Experiment

(ATTREX). In addition to the ATTREX in situ measurements, we use TTL cirrus extinctions retrieved by the Cloud–Aerosol Lidar with Orthogonal Polarization (CALIOP) instrument onboard *CALIPSO* to compare the limited aircraft measurements to a global dataset. We focus on the frequency distributions of cirrus ice concentration, extinction, and ice mass; the TTL cirrus occurrence frequency; and the frequency distribution of relative humidity with respect to ice. In section 2, we revisit the competition between heterogeneous and homogeneous nucleation indicated by parcel model simulations. In section 3, we describe the methodology for simulating TTL cirrus throughout the tropics with a one-dimensional cloud model forced by meteorological analysis fields along trajectories. The ATTREX and CALIOP cirrus and humidity measurements are described in section 4. The results are described in section 5, and section 6 provides a summary and discussion.

2. Parcel model simulations of ice nucleation

Parcel models (also called ''box models'') with zero spatial dimensions have been used to study ice nucleation in a number of past studies (e.g., Kärcher and Ström 2003; Spichtinger and Krämer 2013). The advantages of this approach are the ability to isolate nucleation processes and sensitivities from other cloud processes and computational efficiency. The disadvantage is the lack of realistic treatment of processes such as sedimentation and entrainment that substantially alter cirrus microphysical properties as the clouds age. For example, sedimentation produces fall streaks with much lower ice concentrations than were present in the nucleation layer. Also, for heterogeneous nucleation on IN with a range of threshold supersaturations, sedimentation may remove ice crystals from the nucleation layer before the nucleation event is complete. We begin by reexamining the parcel model indications of dependencies of ice concentration just after nucleation events on mode of nucleation and dynamical forcing.

It is important to emphasize here that the parcel model calculations discussed above only predict the peak ice concentration just after the nucleation event is complete, and they are only representative of the vertical level where ice nucleation occurs. Cloud processes such as sedimentation, entrainment, and aggregation all tend to reduce ice concentrations as the clouds age; in particular, sedimentation fall streaks produce broad regions below the nucleation layer with relatively low ice concentrations (Jensen et al. 2012, 2013a; Murphy 2014). Cirrus measurements generally sample the clouds in a variety of vertical locations and ages. Only in wave clouds is it possible to repeatedly sample the nucleation zone. As a result, the statistics of ice concentrations simulated with parcel models are generally not appropriate for comparison with observed statistical distributions of ice concentration. In the remainder of this paper, we use one-dimensional simulations of TTL cirrus and compare the simulated cloud properties with in situ and remote sensing observations.

a. *Competition between homogeneous and heterogeneous ice nucleation*

As discussed above, at the very low temperatures ($\simeq$180–210 K) prevailing in the TTL, the possible modes of ice nucleation include homogeneous (spontaneous) freezing of aqueous solution drops, heterogeneous freezing of aqueous aerosols on insoluble inclusions, and deposition nucleation directly on the surfaces of dry aerosol particles. The temperature at which homogeneous freezing occurs is primarily a function of the aerosol activity, which is a measure of the solution concentration. In the absence of very rapid temperature changes, the aqueous aerosol water content (activity) remains in equilibrium with the ambient water vapor (Möhler et al. 2003). Therefore, as the air temperature cools and relative humidity increases, the aerosols take up water and dilute until they reach the homogeneous freezing solution concentration. The relative humidity with respect to water at which homogeneous freezing is triggered corresponds to a large supersaturation with respect to ice [critical relative humidity with respect to ice (RHI_{crit}) of $\simeq$165% at TTL temperatures]. Laboratory studies have shown that this homogeneous freezing threshold is essentially independent of the detailed aerosol composition (Koop et al. 2000), which greatly simplifies representation of homogeneous freezing in models. It is worth noting that even small variations in the homogeneous freezing threshold supersaturation with aerosol composition can significantly affect the concentration of ice crystals produced (Murphy 2014), and TTL aerosols are generally multicomponent mixtures, with most aerosols containing organic and inorganic components (Froyd et al. 2009). Such small variations in homogeneous freezing threshold supersaturation would not be discernible in the laboratory experiments with typical temperature and water vapor measurement uncertainties.

Heterogeneous nucleation of ice crystals is much more complicated, with dependencies on the solid particle composition, heterogeneities in composition and surface properties, and the hydroscopicity of the aerosols (Pruppacher and Klett 1997). Both theoretical considerations and laboratory measurements have been used to develop parameterizations of heterogeneous nucleation in models (e.g., Hoose and Möhler 2012),

with primary dependence on relative humidity and temperature. As discussed above, very little is known about the abundance or properties of IN in the TTL. Here, we make the simple assumption that IN present are active whenever the ice saturation ratio s_{ice} exceeds a value of 1.3, and we explore the sensitivity to the number concentration of these IN. The rate of ice nucleation when s_{ice} exceeds 1.3 is assumed to be $1/60\,s^{-1}$. In section 5b, we explore the more realistic situation with a variety of IN types having different nucleation thresholds.

Several past studies have used parcel models to investigate the ice concentration produced by homogeneous freezing events (e.g., Sassen and Dodd 1989; Heymsfield and Sabin 1989; Jensen and Toon 1994; Kärcher and Lohmann 2002). These parcel simulations predict the ice concentration just after completion of a nucleation event. As a parcel cools and the relative humidity increases to the threshold for homogeneous freezing, the largest aerosols will freeze first and begin to grow in the highly supersaturated environment. As cooling continues, nucleation of ice in smaller and smaller aerosols will occur until the ice crystals are abundant enough such that depletion of vapor by deposition growth reverses the increase in relative humidity driven by the cooling. The parcel models show that the concentration of ice crystals produced by homogeneous freezing is strongly dependent on cooling rate, moderately dependent on temperature, and only weakly dependent on aerosol number concentration. The weak dependence on total aerosol number concentration results from the fact that only a small fraction of the aerosol population freezes to produce ice crystals: the aerosol concentration in the upper troposphere is typically 10–1000 cm^{-3}, whereas the ice concentration in cirrus rarely approaches or exceeds $1\,cm^{-3}$ (Jensen et al. 2013a).

Parcel models have also been used to study the competition between heterogeneous and homogeneous ice nucleation in cooling air parcels (e.g., DeMott et al. 1997; Jensen and Toon 1997; Kärcher and Ström 2003; Kärcher 2004; Kärcher et al. 2006; Spichtinger and Cziczo 2010). As discussed above, the presence of heterogeneous IN can modify cirrus properties because IN can be active at supersaturations much lower than those required for homogeneous freezing, thus allowing ice crystals to nucleate earlier in a rising parcel. Also, effective IN comprise a small subset of the upper-tropospheric aerosol population [upper-tropospheric IN concentrations are almost always less than $100\,L^{-1}$ (DeMott et al. 2003)], so the ice concentration in cirrus can be controlled by the abundance of IN if heterogeneous nucleation is the only ice production process occurring and the IN concentration is low relative to typical cirrus ice concentrations. The relative importance of the homogeneous and heterogeneous nucleation processes ultimately depends on the abundance of ice nuclei and the cooling rate. In a slowly cooling parcel with relatively high IN concentrations, growth of ice crystals nucleated on IN at low supersaturation will quench the rising supersaturation before the homogeneous freezing limit (i.e., RHI_{crit}) is reached, and the cloud microphysical properties will depend on IN properties only. In the other extreme, with rapid cooling and relatively few IN, the ice crystals nucleated on IN at low supersaturation are too few to quench the rising supersaturation, and homogeneous freezing will ultimately be triggered when RHI_{crit} is reached, resulting in nucleation of numerous ice crystals. In this case, the cloud properties will primarily be controlled by homogeneous freezing.

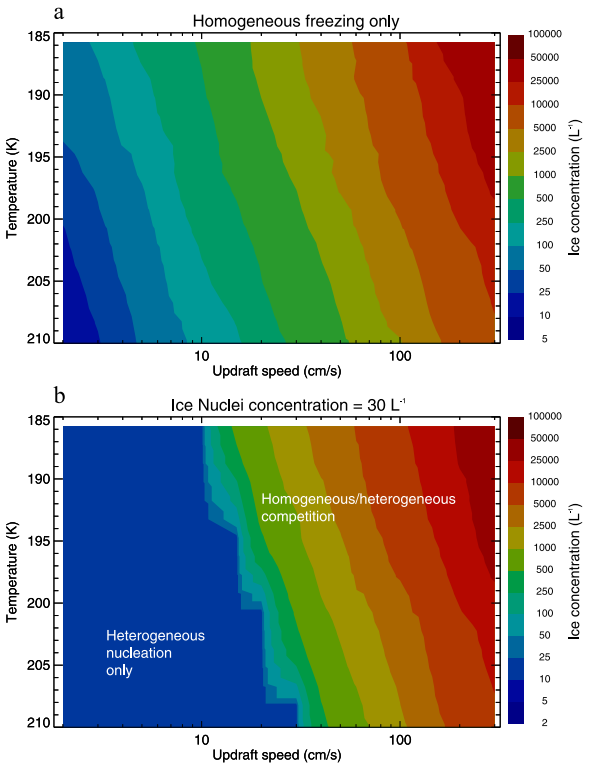

FIG. 1. The number concentration of ice crystals nucleated in a cooling parcel is plotted vs updraft speed (cooling rate) and temperature. (a) Simulations with homogeneous freezing of aqueous aerosols only and (b) including $30\,L^{-1}$ IN active at RHI $\simeq$ 130%. Note that these box model simulations omit sedimentation and only indicate the maximum concentration of ice crystals just after nucleation is complete.

Figure 1 demonstrates the dependence of ice concentration on temperature, cooling rate, and the presence of IN indicated by parcel model simulations. For these box model calculations, we used a model that

tracks the nucleation and growth of individual ice crystals (Jensen and Pfister 2004), with the exception that we are not including sedimentation at this point. Homogeneous freezing nucleation rates as a function of temperature and relative humidity are calculated using the formulation provided by Koop et al. (2000). We assume a lognormal size distribution of aqueous aerosols with a total concentration of $1000\,\mathrm{cm}^{-3}$, a mode radius of $0.01\,\mu\mathrm{m}$, and a distribution width of 2.0. As discussed above, the ice concentration produced by homogeneous freezing is only weakly dependent on the specification of aerosol size distribution (Kärcher and Lohmann 2002). For each aerosol size range, the freezing rate is calculated, and we determine whether new ice crystals should be created in a time step depending on the assumed volume of the parcel and the number concentration of aerosols in the size bin. Once ice crystals are nucleated we track their deposition growth and change the water vapor concentration accordingly.

The strong dependence of ice concentration (i.e., N_{ice}) on cooling rate is apparent in the set of simulations with only homogeneous freezing (Fig. 1a). At TTL temperatures, homogeneous freezing driven by rapid cooling (such as high-frequency gravity waves) can produce ice concentrations well in excess of $1000\,\mathrm{L}^{-1}$. Such large ice concentrations were occasionally observed in narrow layers near the tropical tropopause during the ATTREX campaigns (Jensen et al. 2013b).

As discussed above, heterogeneous nuclei will generally dominate ice production at low cooling rates, where quenching of supersaturation by growth of heterogeneously nucleated ice crystals can prevent homogeneous freezing. Figure 1b shows an example with $30\,\mathrm{L}^{-1}$ IN. The ice concentration is limited to less than $30\,\mathrm{L}^{-1}$ at updraft speeds less than about 10–20 $\mathrm{cm\,s}^{-1}$. Even at somewhat higher updraft speeds (20–30 $\mathrm{cm\,s}^{-1}$), the heterogeneously nucleated ice crystal growth slows the rise in supersaturation and somewhat decreases the ice concentration produced by homogeneous freezing. If higher numbers of IN were present, heterogeneous nucleation would dominate over a broader range of updraft speeds.

b. *Influence of waves on ice nucleation*

Since the dependence of ice concentration on dynamical forcing is strong, this sensitivity must be included in an evaluation of the impact of IN abundance. Parcel model simulations have also been used to investigate the influence of atmospheric waves on cirrus ice nucleation. Upper-tropospheric temperature variability is dominated by waves spanning a wide range of frequencies (from gravity waves with periods approaching the Brunt–Väisälä periods of about 10 min to planetary waves with periods of weeks). Higher wave frequencies and larger wave amplitudes generally drive higher cooling rates and result in higher ice concentrations produced by homogeneous freezing events. The phase of the wave at the location and time where nucleation occurs will also affect cooling rate and ice concentration. In some cases (particularly for very high-frequency waves), the wave-driven temperature reaches a minimum partway through the nucleation event and the parcel starts to warm up, thereby truncating the nucleation event and limiting ice concentration (Jensen et al. 2010; Spichtinger and Krämer 2013; Dinh et al. 2016). The result is that the variety of wave frequencies, amplitudes, and phases present in the TTL can produce a wide range of ice concentrations even if homogeneous freezing is the only ice production process (Kärcher and Ström 2003). Note that, although we are not including the high-frequency wave nucleation-quenching effect in the parcel model simulations discussed above, this effect is included in the full trajectory-curtain simulations with wave spectra described below.

3. Global simulations of TTL cirrus

Following Jensen and Pfister (2004) and Ueyama et al. (2014, 2015), we use a semi-Lagrangian model to simulate cirrus throughout the TTL. The first step is to run a large number of diabatic back trajectories from a uniform grid in the tropics. For the cloud simulations discussed here, we use the set of trajectories described by Ueyama et al. (2015): 60-day back trajectories ending on 1 February 2007 every 2° longitude × 2° latitude spanning the tropics (20°S–20°N) at 372-K potential temperature (approximately 100-hPa pressure). Wind fields and temperatures are based on the European Centre for Medium-Range Weather Forecasts interim reanalysis (ERA-Interim; Dee et al. 2011). Next, we extract vertical profiles of temperature from each time and location along each trajectory, thus generating "curtains" of temperature versus potential temperature and time. These temperatures are then used (stepping forward in time) to drive a one-dimensional cloud model that treats homogeneous freezing of aqueous aerosols, heterogeneous ice nucleation on solid particles, ice crystal deposition growth and sublimation, ice crystal sedimentation, and vertical advection of ice crystals. The cloud model is Lagrangian in that we track the size and location of thousands of individual ice crystals to represent the cloud (see Jensen and Pfister 2004). This approach avoids the numerical diffusion and dispersion associated with Eulerian treatments of advection (either in the ice crystal size dimension or the vertical dimension). Ice crystal aggregation is not treated, but high-resolution ice crystal images from ATTREX

suggest very few aggregates are present in TTL cirrus (S. Woods 2016, personal communication). Water vapor is treated with an Eulerian vertical grid spanning 350–430-K potential temperature with 200 levels (0.4-K vertical spacing). The vapor lost or gained by growing/sublimating ice crystals is calculated by summing the change in size of all ice crystals within each vertical grid box over the time step. The water vapor vertical profile for each trajectory curtain is initialized using measurements from the Microwave Limb Sounder (MLS; Read et al. 2007).

The TTL vertical motion field in balance with radiative heating is important, particularly for simulating water vapor concentration (Ueyama et al. 2015). Above about 150 hPa, the diabatic heating is dominated by radiative heating, and other terms in the thermodynamic equation (such as latent heating) are negligible (Wright and Fueglistaler 2013). Therefore, we can diagnose the diabatic vertical motion from the radiative heating. Given the strong dependence of TTL radiative heating on clouds (both within and below the TTL) and the large uncertainties in representations of clouds in global models, the radiative heating rates and corresponding diabatic ascent rates in the analysis models are necessarily uncertain. We prefer to use the Yang et al. (2010) offline calculations based on satellite observations of cloud fields. The disadvantage of this approach is that the Yang et al. (2010) calculations are only available as monthly averages, given the need to average the sparse satellite cloud measurements. In reality, the heating rates and vertical motions no doubt vary on much shorter time scales indicated by the highly variable cloud fields. Ueyama et al. (2015) showed that high-frequency variability does not seem to have an overwhelming effect, at least for the global patterns of TTL cirrus and water vapor averaged over several days. An additional limitation of using the radiative heating rates calculated offline is that they are only available for the 2006/07 winter, whereas the ATTREX data were collected in late winter, 2014. We use CALIOP data to investigate the magnitude of interannual variability in TTL cirrus microphysical properties (see section 5).

Another key requirement for proper simulation of TTL cirrus is accurate representation of temperature variability. As discussed above, waves on a variety of scales dominate TTL temperature variability. Even modern reanalyses lack the temporal and spatial resolution required to resolve all of the important wave scales. Kim and Alexander (2013) developed an approach for proper interpolation of the wave spectral components between model levels. In addition, Kim and Alexander (2013) provided amplification factors based on comparisons with tropical radiosondes to account for the underrepresentation of wave amplitudes in the analysis.

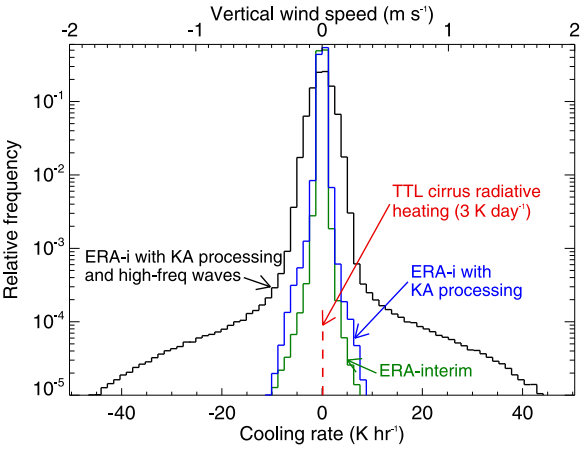

FIG. 2. Frequency distributions of TTL cooling rate along isentropes are shown. The corresponding range of adiabatic vertical wind speeds (assuming a temperature lapse rate of 7 K km^{-1}) is shown on the top axis. The distribution directly from ERA-Interim fields (green curve) is relatively narrow, with vertical wind speeds no larger than about 20 cm s^{-1}. Applying the wave interpolation and amplification (based on radiosondes) scheme of Kim and Alexander (2013) (KA; blue) broadens the distribution slightly. Superimposing high-frequency waves based on the parameterization discussed by Jensen and Pfister (2004) results in much larger vertical wind speeds. Note that vertical wind speeds approaching or exceeding 1 m s^{-1} still occur rarely. The dashed red line shows a typical value of TTL cirrus cloud radiative heating (3 K day^{-1} = 0.125 K h^{-1}, corresponding to about 0.5 cm s^{-1} vertical wind speed).

Last, we use the parameterization developed by Jensen and Pfister (2004) (based on TTL wave observations) to superimpose waves with periods of less than two cycles per day that cannot be resolved in the 6-hourly analysis output fields. Ueyama et al. (2015) compared the ERA-Interim temperature fields (including these wave adjustments) with tropical radiosondes and found that biases in the cold-point temperature were no more than 0.3 K. The accurate representation of TTL temperatures and wave motions represents a significant advance over past trajectory studies of TTL cirrus and water vapor.

Figure 2 shows frequency distributions of cooling rate along isentropic surfaces for the temperature fields used in the simulations. Corresponding adiabatic vertical wind speeds are shown assuming a lapse rate of 7 K km^{-1}. The global analysis models (in this case ERA-Interim) are limited to cooling rates of less than 5–10 K h^{-1} (vertical wind speeds less than 20–30 cm s^{-1}). Applying the Kim and Alexander (2013) scheme to properly interpolate and amplify the waves in ERA-Interim wind and temperature fields broadens the vertical wind speed frequency distribution somewhat. The addition of high-frequency (less than 2 cycles per day) waves using the parameterization described by Jensen

and Pfister (2004) results in much larger cooling rates along the trajectories. It should be noted that the rapid cooling events (vertical wind speed $w \geq 50\,\mathrm{cm\,s^{-1}}$) occur relatively infrequently, which is consistent with the infrequent occurrence of very high concentrations of ice in TTL cirrus (see discussion of TTL cirrus simulations below). We note here that the wave parameterization used is an attempt to represent climatological-mean temperature variability driven by waves. In reality, the wave amplitudes and frequencies are highly variable in space and time, with stronger wave activity near sources such as orography and deep convection.

Also shown in Fig. 2 is a typical value of TTL cirrus cloud radiative heating ($3\,\mathrm{K\,day^{-1}} = 0.125\,\mathrm{K\,h^{-1}}$, corresponding to about $0.5\,\mathrm{cm\,s^{-1}}$ vertical wind speed) (Jensen et al. 1996; Comstock et al. 2002; Dinh et al. 2010). The cloud radiative heating is dwarfed by even synoptic-scale temperature variability that is ubiquitous in the TTL. Therefore, under typical conditions, effects of this cloud radiative heating on temperature and stability will be swamped by wave-driven heating/cooling.

As discussed above, the highest-frequency gravity waves (periods approaching the Brunt–Väisälä period of about 10 min in the upper troposphere) can actually quench nucleation if the temperature starts to warm up before a nucleation event is complete. This effect is included in the simulations presented here; however, the impact on ice concentrations is small, because the wave amplitudes of the highest-frequency components in our wave spectrum are small. As described by Jensen and Pfister (2004), the power spectrum of wave energy versus frequency is assumed to follow an $\hat{\omega}^{-2}$ power law, where $\hat{\omega}$ is the intrinsic frequency, such that the amplitude of temperature oscillations at the high frequencies is small (<0.05 K).

Yet another key factor affecting TTL cirrus and humidity is deep convection penetrating into the TTL. A number of past studies have shown that deep convection is either directly or indirectly responsible for much of the TTL cloudiness (Pfister et al. 2001; Massie et al. 2002; Riihimaki and McFarlane 2010; Riihimaki et al. 2012). Detrainment of ice from deep convection can either hydrate or dehydrate the TTL, depending on the ambient relative humidity where the ice detrains (Jensen et al. 2007). Ueyama et al. (2014) showed that convection predominantly hydrates the TTL, with increases in lower TTL water vapor concentration of 1–5 ppmv. The contribution of ice detrained directly from deep convection to TTL cirrus is unclear. Ice crystal images in tropical cirrus even relatively close to active deep convection typically suggest a predominance of bullet rosette habits (Whiteway et al. 2004) (see also S. Woods 2016, personal communication), indicative of in situ ice nucleation and/or growth in the upper troposphere. In contrast, in anvil cirrus detrained directly from deep convection, irregular aggregate habits generally predominate (Lawson et al. 2006a). Further, the occurrence frequency of convection extending into the TTL decreases rapidly with height above ≃13–14 km (Ueyama et al. 2015). We assume here that the microphysical properties of uppermost tropospheric cirrus are dominated by in situ formed clouds that are treated by our model.

Regardless of whether ice detrained directly from deep convection contributes a great deal to TTL cirrus, the TTL hydration by deep convection will undoubtedly lead to in situ cirrus formation downstream of the convection in colder regions of the tropics. We treat the influence of deep convection on TTL humidity by tracing the trajectories through 3-hourly geostationary satellite fields of infrared cloud top and rainfall (see Pfister et al. 2001; Bergman et al. 2012; Ueyama et al. 2014 for details). Whenever a trajectory passes through deep convection extending into the TTL, we saturate the column model up to the potential temperature corresponding to the cloud top. The convective cloud-top heights have been adjusted to account for biases in the infrared retrievals of cloud-top altitude.

As a parcel makes its 1–2-month journey upward through the TTL, several cloud formation events typically occur. Assuming heterogeneous IN promote the ice nucleation, the most effective IN will be scavenged by sedimentation of the ice crystals. Without IN replenishment, the IN population is mostly removed from the TTL well before the end of our 60-day curtain simulations. Detrainment from deep convection would seem to be the most likely source of IN to the TTL; however, the abundance of IN in convective outflow is not known. Many of the effective IN may participate in ice formation at lower levels in the deep convection and be removed by sedimentation of the ice crystals. In the absence of any information about TTL IN sources, we make the simplified assumption here that, whenever convective influence on the trajectory curtain occurs (see above), the IN population is restored to the assumed initial abundance.

Figure 3 shows the time evolution of clouds forming in the first few days of a representative simulation. In this case, we assumed $30\,\mathrm{L^{-1}}$ IN effective at $s_{\mathrm{ice}} > 1.3$. This example shows a number of features that are typical of TTL cirrus simulated with the temperature-curtain approach: 1) heterogeneous nucleation occurs in more locations than homogeneous freezing; 2) supersaturations approaching the threshold for homogeneous freezing (and homogeneous freezing events themselves) occur in small patches, and the large supersaturations are rapidly quenched by growth of numerous ice crystals nucleated; 3) the localized homogeneous freezing events produce narrow layers with high ice concentrations embedded in

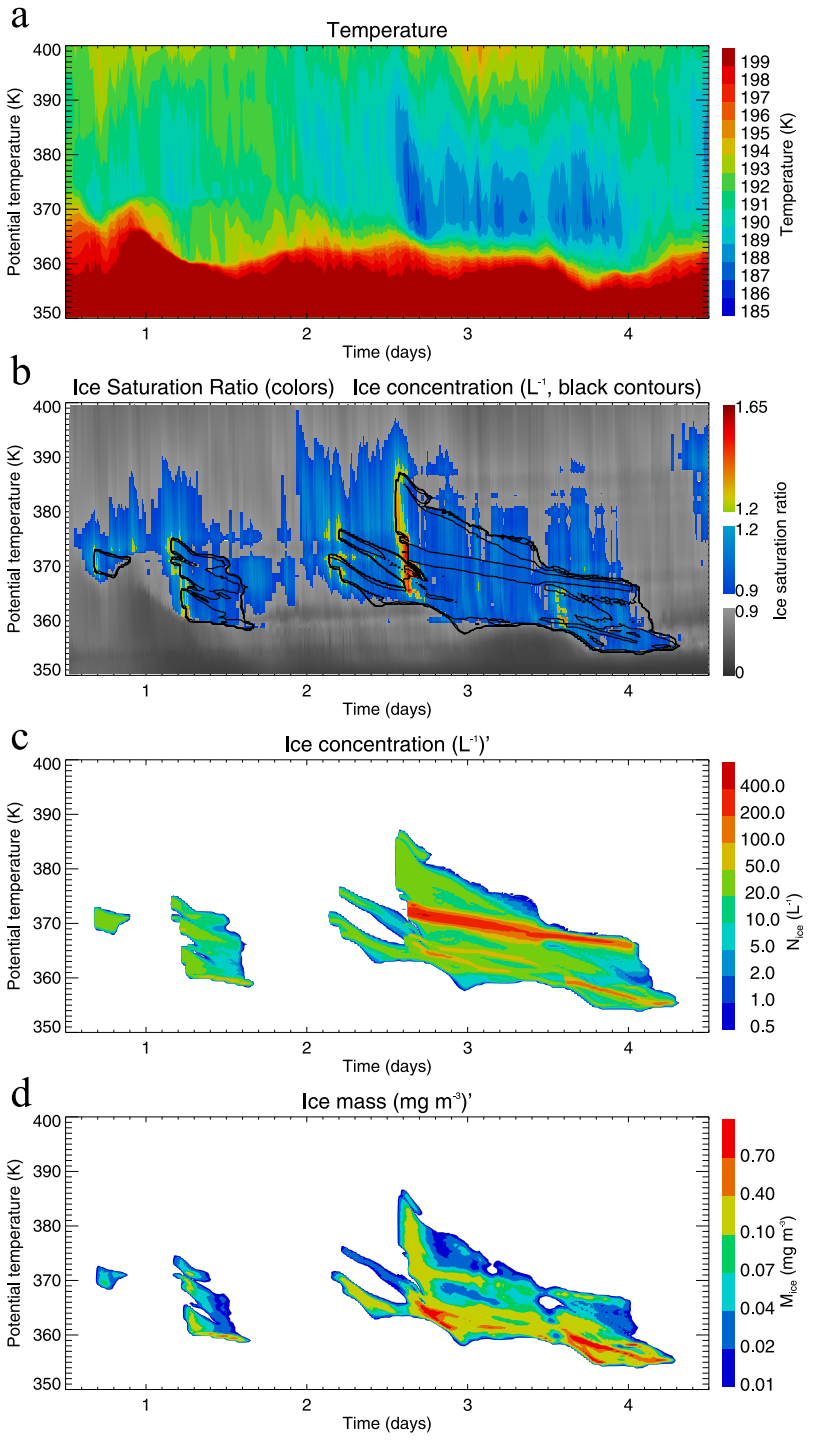

FIG. 3. A representative example of a segment of one of the temperature-curtain simulations of TTL cirrus is shown. (a) Temperature, (b) ice saturation ratio, (c) ice concentration, and (d) ice mass vs time and potential temperature. Black contours in (b) also show ice concentration contours to indicate where the cloud outlines are relative to the supersaturated regions. We have assumed 30 L^{-1} ice nuclei effective at a ice saturation ratio of 1.3 in this case. Only heterogeneous nucleation occurs in the first cloud patch at about 1.3 days and through most of the depth of the cloud forming later at about 2.2–4 days. Homogeneous nucleation occurs in a few narrow layers where the cooling rate is high enough to drive up supersaturation even after ice crystals have nucleated on the IN such that the threshold for homogeneous freezing ($s_{ice} \simeq 1.65$) can be reached. These homogeneous freezing events produce narrow layers of relatively high ice concentrations (up to about 500 L^{-1} in this case).

deeper cloud layers with low ice concentrations (Fig. 3c), consistent with the ATTREX observations (Jensen et al. 2013b); 4) sedimentation of ice from the narrow high-concentration layers generates deep layers with relatively low ice concentrations; 5) the slopes of cloud layers in time–height space are steeper for heterogeneously nucleated cloud layers (fewer, larger ice crystals falling faster) than for homogeneously nucleated layers (more numerous, smaller ice crystals falling slower); 6) individual cloud elements persist no longer than 1–2 days; 7) the trailing edges of the cloud are collocated with temperature increases (i.e., cloud dissipation is typically driven by temperature variability).

The semi-Lagrangian, one-dimensional cirrus modeling approach used here does not permit inclusion of interactions between radiative heating, small-scale dynamics, and cloud processes. Dinh et al. (2010, 2012, 2014) have shown that mesoscale circulations driven by cloud radiative heating can, under some circumstances, help maintain TTL cirrus and increase the vertical transport of water vapor. Also, if the clouds persist long enough, entrainment and mixing will reduce ice concentrations (Jensen et al. 2012). On the other hand, the radiative heating rates in TTL cirrus are relatively weak compared to wave-driven temperature variability (see Fig. 2), and the time scale for thermal instability to build up is on the order of a day. Determining cloud lifetimes from ground-based, airborne, or satellite measurements is generally not possible because the observations only provide snapshots of cloud properties. Ground-based lidar observations may suggest long-lived TTL cirrus; however, the persistence of cloud layers in the lidar data could just be indicative of air advecting through a stationary cold pool conducive to cloud formation, and the lifetime (following the flow) of individual cloud elements may be relatively short. The trajectory-curtain modeling approach suggests that TTL cirrus cloud elements typically last no longer than about 12–48 h (Jensen et al. 2011), which is only marginally long enough for significant radiatively driven circulations to begin to develop. As in the example shown in Fig. 3, the lifetime of individual cloud elements is typically limited by wave-driven temperature increases that lead to sublimation of the ice crystals. We suggest that radiatively driven motions likely have second-order impacts on TTL cirrus microphysical properties under typical conditions.

4. Measurements of TTL cirrus microphysical properties and relative humidity

Before presenting the statistical properties of TTL cirrus simulated with our global temperature-curtain simulations, we first discuss the ATTREX water vapor, temperature, and cloud measurements, as well as the CALIOP extinction and cloud frequency measurements, which we use to evaluate the simulations. ATTREX included three flight series. For the first two flight series in October–November 2011 and January–March 2013 the Global Hawk was based at Armstrong Flight Research Center (AFRC) in Southern California. The long range of the Global Hawk permitted extensive sampling in the tropics despite the midlatitude location of AFRC. In 2014, the aircraft was deployed to Guam in the western Pacific, and six flights were flown out of Anderson Air Force Base during February and March. We focus here on the flights from Guam because the aircraft had the most extensive cirrus microphysics instrumentation during this deployment. See Jensen et al. (2015) for details on the ATTREX Guam objectives, payload, flights, and measurements.

The TTL cirrus measurements used here were made with the Spec Inc. Hawkeye probe [see S. Woods (2016, personal communication) for details of the ATTREX cirrus observations]. Hawkeye is a combination of two imaging instruments [equivalent to the two-dimensional stereo (2D-S) probe (Lawson et al. 2006b) and the Cloud Particle Imager (CPI; Lawson et al. 2001)], as well as a spectrometer [equivalent to the fast cloud droplet probe (FCDP)]. The FCDP measures the forward scattered laser light from individual cloud particles and infers the size of particles from 2- to 50-μm diameter (McFarquhar et al. 2007). The 2D-S probe is an optical array imager that captures images of ice crystals with sizes ranging from 10 μm to 4 mm. The CPI provides detailed ice crystal images that can be used to determine habit information for crystals with maximum dimensions larger than about 40 μm. For the purpose of this study, we use ice crystal concentrations from FCDP and 2D-S as well as extinctions and ice mass contents from 2D-S. We do not use FCDP extinction or ice mass measurements because sizing of nonspherical ice crystals by FCDP is uncertain. Extinction is a direct measurement for 2D-S and ice mass is determined using area-to-mass relationships (Baker and Lawson 2006). All ice crystal probes flown on high-speed jet aircraft are subject to shattering artifacts that can inflate the measured concentrations of small crystals. The Hawkeye data processing includes interarrival time analysis for identification and removal of shattering artifacts (Baker et al. 2009; Lawson 2011). In any case, TTL cirrus generally contain too few large crystals to produce significant numbers of shattering artifacts compared to the concentrations of natural small crystals (Lawson et al. 2008).

The CALIOP instrument onboard *CALIPSO* has been providing a wealth of information about upper-tropospheric cirrus microphysical properties and

occurrence frequencies on a global scale since 2006 (Anselmo et al. 2007). The direct measurement made by CALIOP is attenuated backscatter; calculation of extinction requires assumptions about the extinction-to-backscatter ratio, which varies with particle size (Young and Vaughan 2009). Yang et al. (2010) independently estimated the CALIOP extinction uncertainty to be about 30%. Here, we use the CALIOP level 2 cloud layer and cloud profile measurements (version 3.1 for 2007 and version 3.3 for 2014). The extinction data are screened to exclude integrated attenuated backscatter values less than 0.001 and greater than 0.019 to avoid noise problems on the low end and optically thick convective clouds on the high end. Our TTL cirrus simulation approach does not include ice crystals detrained directly from deep convection, and such clouds were rarely sampled during ATTREX.

We also use the measured statistical distributions of relative humidity with respect to ice to evaluate our simulations of TTL cirrus. The challenge of measuring water vapor under the extremely dry TTL conditions (H_2O mixing ratios as low as 1 ppmv) was addressed by ATTREX with two complementary instruments flown on the Global Hawk. The NOAA Water (NW) instrument provides a closed-cell tunable-diode laser (TDL) measurement that includes the in-flight calibration system used on the NOAA chemical ionization mass spectrometer (CIMS) instrument during the Mid-Latitude Airborne Cirrus Properties Experiment (MACPEX; Thornberry et al. 2015). The NW instrument also measures total water concentration using a forward-facing inlet that enhances ice concentration in the sample flow by operating subisokinetically. The diode laser hygrometer (DLH) instrument provides an open-path TDL measurement by firing the laser from the fuselage to a reflector on the wing and measuring the return signal. The pathlength (12.2 m) is long enough to provide a precise, fast measurement of water vapor. Temperature, pressure, and wind measurements were made with the meteorological measurement system (MMS). The combined uncertainties in MMS temperature (0.3 K) and H_2O from DLH or NW (5%–10%) result in an uncertainty in derived RHI of no more than about 15%.

We note here that past measurements of water vapor concentration under these dry conditions have been plagued by large, unresolved discrepancies between different instruments (Oltmans and Rosenlof 2000; Weinstock et al. 2009). We have a high level of confidence in the estimated accuracy of the DLH and NW measurements ($\simeq$5%–10%) for two reasons: 1) The NW and DLH data obtained on the 2013 and 2014 flights suggest a high degree of consistency and agreement for TTL H_2O values less than 10 ppmv (T. Thornberry et al. 2016, unpublished manuscript). 2) In TTL cirrus with very high ice concentrations (in excess of 1000 L^{-1}) the relative humidity with respect to ice is consistently near 100% (Jensen et al. 2013b). The time scale for quenching of supersaturation/subsaturation by ice crystal growth/sublimation in such clouds is a few minutes or less such that the RHI is expected to remain near 100%.

Figure 4 shows comparisons between frequency distributions of ice concentration, extinction, and ice water content measured with different instruments. The ice number concentration frequency distributions based on FCDP and 2D-S (Fig. 4a) are very similar, except that the FCDP data indicate ice concentrations larger than a few thousand per liter in some cases, whereas clouds with concentrations greater than about 2000 L^{-1} are not detected by 2D-S. Given the limited available water vapor for deposition growth of TTL ice crystals, the majority of ice crystals in such high-concentration clouds would be no larger than a few micrometers in diameter, which is below the detection threshold for 2D-S. The high-concentration TTL cirrus occur very rarely, and the mean ice concentrations indicated by ATTREX FCDP and 2D-S measurements, Forward Scattering Spectrometer Probe measurements reported by Krämer et al. (2009) and in the numerical simulations (discussed below) are consistently less than about 200 L^{-1}. The FCDP statistics of ice number concentration from ATTREX in 2013 (central and western Pacific) are similar to those from ATTREX in 2014 (western Pacific).

The statistics of TTL cirrus extinction measured by 2D-S and CALIOP (Fig. 4b) are consistent within the uncertainties of the measurements. Sampling biases likely account for some of the differences. The Global Hawk could only reach the tropical tropopause near the end of the Guam flights. As a result, the lower-middle TTL were sampled more frequently than the uppermost TTL, possibly resulting in a high bias in extinction relative to the uniformly sampled CALIOP dataset. Also, despite the fact that the ATTREX 2014 Global Hawk flights provided about 34 h of TTL cirrus sampling, the aircraft data still represent a relatively small sample. We also compare the CALIOP TTL cirrus extinction statistics between the ATTREX 2014 western Pacific TTL and all longitudes during the ATTREX 2014 time period, and the differences are relatively small, consistent with the apparent lack of regional variability in TTL cirrus ice concentrations. Last, we include a CALIOP TTL extinction frequency distribution from 2007 (the year corresponding to the simulations discussed below). The interannual variability in TTL cirrus extinction statistics also seems to be small compared to the measurement uncertainties.

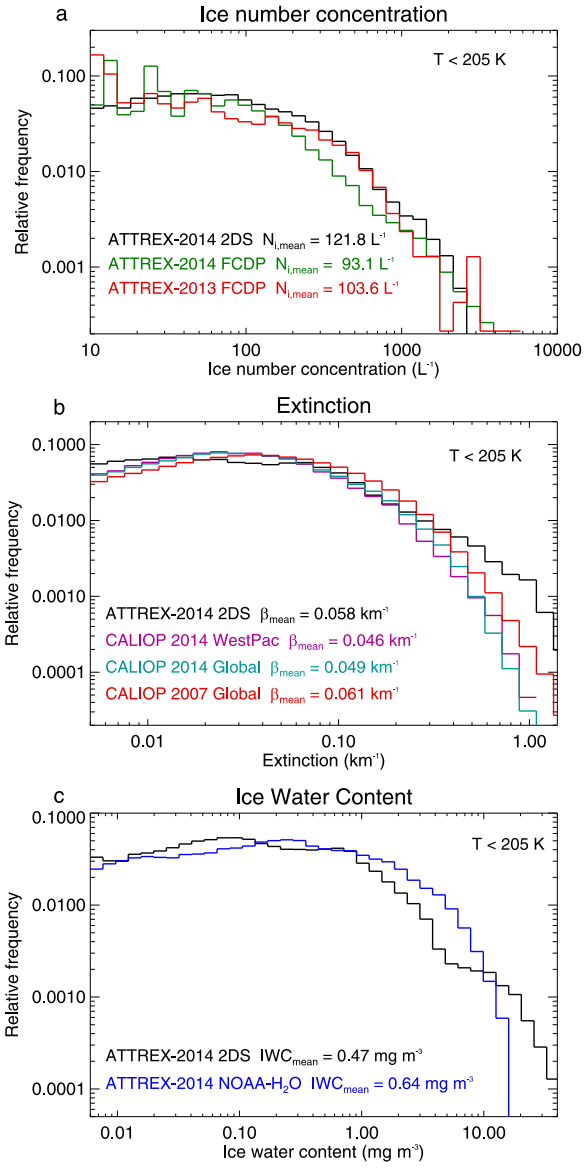

FIG. 4. Frequency distributions of TTL cirrus microphysical properties based on different measurements are compared. (a) Ice crystal number concentration measured by 2D-S and FCDP in ATTREX 2014 (western Pacific) and by FCDP in ATTREX 2013 (central and eastern Pacific); (b) extinctions from ATTREX 2014 2D-S measurements, CALIOP in the region and time period sampled by the Global Hawk during ATTREX 2014, global TTL CALIOP measurements in February–March 2014, and global TTL CALIOP measurements in February–March 2007; (c) ice water content from ATTREX 2014 2D-S and NOAA-H_2O measurements.

The ATTREX 2014 Global Hawk flights provided two measures of ice water content (IWC): from 2D-S (with the aid of mass–dimensional relationships) and from the forward-facing inlet on the NOAA-H_2O instrument. The NOAA-H_2O forward-facing inlet, which

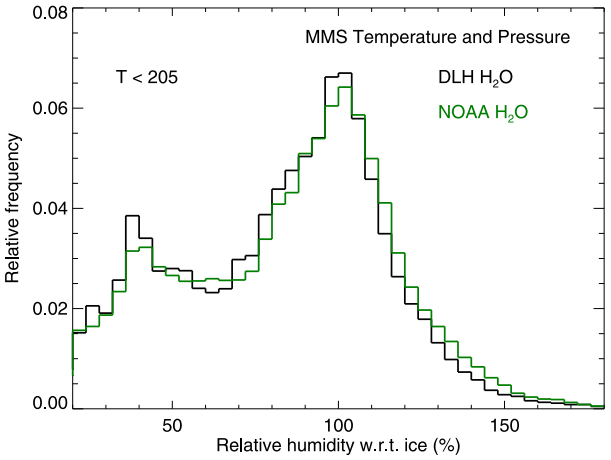

FIG. 5. Frequency of relative humidity with respect to ice in the upper TTL ($T < 205$ K) based on DLH and NOAA-H_2O measurements are shown. The agreement in TTL RHI statistics from the two datasets is excellent. The distributions show the expected peak near RHI = 100% (within cirrus) and frequency occurrence of substantial supersaturation with respect to ice.

samples both water vapor and cloud particles, operates subisokinetically, with ice crystals larger than about 8 μm enhanced by about a factor of 40, resulting in a detection limit of about 2 $\mu g\,m^{-3}$ (Thornberry et al. 2015). The agreement between these datasets (Fig. 4c) is reasonably good, certainly indicating consistency within the uncertainties of the measurements. Since cirrus ice mass is generally concentrated in larger crystals, the habits of relatively large TTL cirrus ice crystals assumed in the mass–dimensional relationships will strongly affect the retrieved IWC from 2D-S. The available information about TTL cirrus ice crystal habits prior to ATTREX was limited, and the mass–dimensional relationships could be improved with the extensive ATTREX CPI dataset.

Frequency distributions of TTL relative humidity with respect to ice from the DLH and NOAA-H_2O measurements are compared in Fig. 5. As shown in the detailed analysis of ATTREX water vapor measurements (T. Thornberry et al. 2016, unpublished manuscript), the agreement between DLH and NOAA-H_2O TTL H_2O measurements was generally excellent. Both datasets indicate a peak in the RHI frequency distributions near 100%, corresponding primarily to measurements inside cirrus where the deposition growth/sublimation of ice crystals tends to keep the RHI near ice saturation. Both datasets indicate the relatively common occurrence of substantial supersaturation with respect to ice in the TTL. However, supersaturations approaching the threshold for homogeneous freezing (160%–170% at TTL temperatures) occur relatively infrequently.

TABLE 1. Summary of results from TTL cirrus simulation sensitivity tests. Values are averages for temperatures less than 205 K. The first three rows show measured values. Variables $f_{ice,het}$, $f_{\beta,het}$, and $f_{IWC,het}$ are the fractions of TTL cirrus ice number, extinction, and mass in ice crystals nucleated heterogeneously. Variable $s_{i,nuc}$ is the assumed saturation threshold for activation of heterogeneous nuclei.

Case	$N_{ice,mean}$ (L^{-1})	β_{mean} (km^{-1})	IWC_{mean} ($mg\,m^{-3}$)	$f_{ice,het}$	$f_{\beta,het}$	$f_{IWC,het}$	Cloud fraction (16–18 km)
Measurements							
ATTREX 2D-S	122	0.058	0.47	—	—	—	—
CALIOP Jan 2007 (global)	—	0.056	—	—	—	—	0.13
CALIOP Jan 2007 (west Pacific)	—	0.046	—	—	—	—	0.13
Model results							
Homogeneous freezing only	290	0.069	0.30	0	0	0	0.15
No. high-frequency waves	115	0.039	0.25	0	0	0	0.081
$N_{IN} = 30\,L^{-1}$, $s_{i,nuc} = 1.3$	198	0.053	0.26	0.002	0.05	0.19	0.17
$N_{IN} = 100\,L^{-1}$, $s_{i,nuc} = 1.3$	145	0.050	0.26	0.05	0.29	0.50	0.17
$N_{IN} = 300\,L^{-1}$, $s_{i,nuc} = 1.2$–1.6	111	0.44	0.25	0.17	0.49	0.71	0.18

Any precision limitation of the temperature and water vapor measurements will tend to broaden the ice saturation ratio frequency distribution. The estimated precision of the DLH H_2O measurement is 50 ppbv + 0.1% for 1-Hz data, and the MMS temperature and pressure precisions are approximately 0.003 hPa and 0.05 K, respectively. The resulting ice saturation ratio precision is no worse than about 0.02; thus, the precision-driven scatter in measurements should not contribute significantly to the width of the ice saturation ratio distribution.

5. Results

We have run several experiments with the trajectory-curtain model. Each experiment consists of 3780 individual simulations along back trajectories ending in a uniform grid across the tropics. We begin with homogeneous freezing only (no IN available) and run sets with and without the Kim and Alexander (2013) wave interpolation/amplification and superposition of high-frequency waves. Next, we include heterogeneous ice nuclei with threshold ice saturation ratios of 1.3 and abundances of 30 and 100 L^{-1}. Last, we consider a more plausible scenario with a variety of heterogeneous ice nuclei such that the concentration of active IN increases as ice saturation ratio increases from 1.2 to 1.6. The sets of simulations and statistics of simulated TTL cirrus microphysical properties are listed in Table 1.

a. *The sensitivity of TTL cirrus to dynamical variability*

Comparisons between frequency distributions of 2D-S cloud properties and simulated TTL cirrus microphysical properties with homogeneous freezing only are shown in Fig. 6. We only include ice concentrations less than 3000 L^{-1} in the mean calculation because upper-TTL cirrus with higher ice concentrations are likely composed of ice crystals with sizes below the 2D-S detection limit (5 μm). (A monodispersed cloud containing 2 ppmv of ice with an ice concentration of 3000 L^{-1} at 100-hPa pressure and 195-K temperature will have ice crystal diameters of about 5 μm.) Among the dynamical and microphysical processes considered in this study, temperature variability has the largest effect on TTL cirrus microphysics. Inclusion of gravity waves not represented in the analysis more than doubles the mean ice number concentration. Without the high-frequency waves, the simulated ice concentrations are lower than indicated by the 2D-S dataset. With the full spectrum of waves and homogeneous freezing as the only ice production process, the model produces excessively high ice concentrations by a rather wide margin. Even in a set of simulations with the high-frequency wave amplitudes decreased by a factor of 2 (not shown), the ice concentrations are nearly a factor of 2 larger than indicated by the observations. However, as also noted above, even a small dependence of the threshold for homogeneous freezing on variations in aerosol composition could significantly reduce the number of ice crystals nucleated (Murphy 2014). Our assumption that all aqueous aerosols have the same homogeneous freezing threshold produces the largest possible ice concentrations.

We note here that even in the set of simulations without high-frequency waves, high ice concentrations occur on some occasions (red curve in Fig. 6a). These large ice concentrations are an artifact of the temperature-curtain approach we are using. The temperature variability is only correctly following the flow at the vertical level corresponding to the steering trajectory used to generate the curtains. Above and below this level, the curtain is actually crossing the streamlines, which can generate spurious temperature variability that ultimately results in

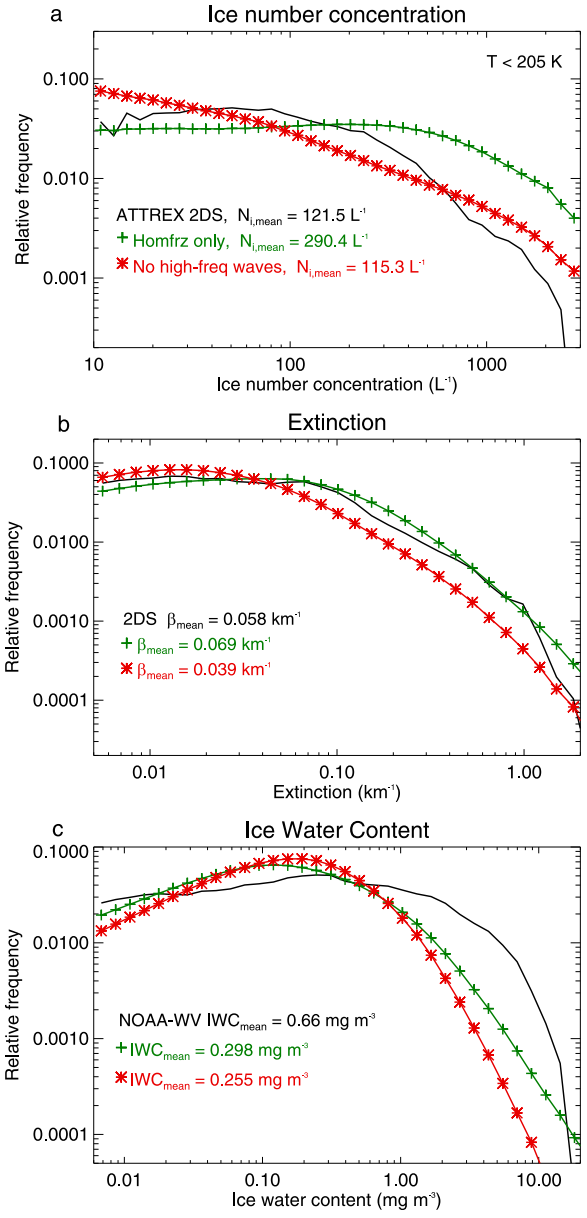

FIG. 6. The 2D-S distributions of ice concentration and extinction, and the NOAA-H_2O ice water content are compared with results from sets of simulations, including only homogeneous freezing ice nucleation and with (green) or without (red) high-frequency waves. Addition of high-frequency waves increases ice concentrations and extinctions, as expected. The simulation without waves seems to overestimate ice concentrations, but the observed distribution of extinction measured by 2D-S is reproduced well. Exclusion of waves results in substantial underestimates of ice number concentration and extinction.

large ice concentrations produced by homogeneous freezing. In reality, these high ice concentrations probably would not be present in simulations properly driven by the analysis temperature variability alone. This spurious temperature variability is swamped by the temperature variability driven by high-frequency waves; therefore, it shouldn't affect the results in the simulations with the high-frequency waves included.

The shape of the extinction frequency distribution in the set of simulations with waves agrees well with the observations, although the mean extinction from the model is somewhat larger than indicated by the 2D-S and CALIOP measurements. The simulated extinctions without high-frequency waves are considerably lower than the observed values. The model seems to overemphasize midrange ice mass values (between about 0.05 and 1 mg m^{-3}), and the model underestimates the mean mass of TTL cirrus by more than a factor of 2 even in the simulation with waves (Fig. 6). It is possible that the largest observed ice water contents are associated with convectively generated cirrus, which are not included in the model.

Next, we examine the impact of dynamical variability on the occurrence frequency of TTL cirrus. Following Ueyama et al. (2015), we examine both the regional distribution and the tropical-average height profile of TTL cirrus occurrence frequency. For these comparisons, we average the model results over the last 30 days of the trajectory-curtain simulations (essentially the month of January 2007), and the CALIOP data are averaged over the same time period. We exclude CALIOP cloud layers for which the 532-nm integrated attenuated backscatter is less than 0.001 (to avoid noise) or greater than 0.019 (to avoid convective clouds). Note that the backscatter upper limit will not remove aged anvil cirrus produced by convection. The tropical-mean (±20° latitude) vertical profiles of cirrus occurrence frequency from simulations with homogeneous freezing and with and without small-scale waves are compared with CALIOP measurements in Fig. 7. As shown by Davis et al. (2010), the most optically thin TTL cirrus are below the detection limit of the CALIOP space-based lidar. For the case with high-frequency waves included, we show the frequencies of both all cirrus in the model and only those with extinctions greater than the 0.005-km^{-1} CALIOP detection threshold. All subsequent model cloud frequencies shown include only the CALIOP-detectable extinctions. The model generally reproduces the observed cloud frequencies and the decrease in cloud frequency with height in the TTL. However, the occurrence of cirrus in the uppermost TTL is underestimated by the simulations even when high-frequency waves are included. Without high-frequency waves, the cloud frequency is much too low throughout the TTL.

The regional distributions of upper TTL (between 16- and 18-km pressure altitude) cloud coverage from

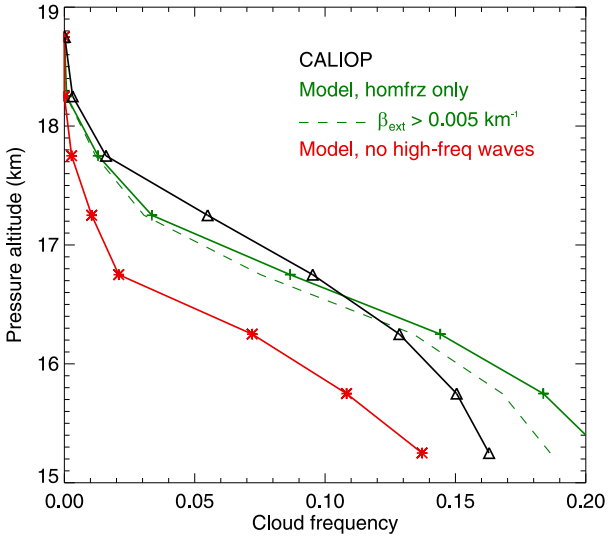

FIG. 7. Tropical-average ($|\text{lat}| < 20°$) cloud frequencies are plotted vs pressure altitude. The different curves show CALIOP January 2007 data (black), simulations with homogeneous freezing only and high-frequency waves included (green), homogeneous freezing simulations with extinctions less than 0.005 km^{-1} excluded (green dashed), and simulations without high-frequency waves included (red). The model cloud frequencies include the last 30 days of the 60-day trajectory-curtain simulations, corresponding to the January 2007 CALIOP measurements.

homogeneous freezing-only simulations with and without waves are compared with the CALIOP measurements in Fig. 8. The overall pattern of TTL cirrus occurrence indicated by CALIOP is reproduced reasonably well by the model including high-frequency waves, although the peak in simulated cloud coverage over the western Pacific is shifted southward and is broader relative to the observations. This offset is presumably related to errors in the temperature variance distributions in ERA-Interim. The model also underestimates the occurrence of cirrus over southern Africa and South America. These continental regions both have deep convection reaching the upper TTL, some of which is likely included in the CALIOP statistics despite our use of an integrated attenuated backscatter upper limit. The simulations without high-frequency waves underestimate cloud occurrence frequencies throughout the tropics.

The comparison between simulated and observed frequency distribution of TTL ice saturation ratio is shown in Fig. 9. With only wave motions resolved by ERA-Interim, the model overestimates the occurrence of RHI greater than about 120% indicated by the ATTREX measurements. With high-frequency waves included, the model substantially underestimates the occurrence of ice supersaturations ranging from about 10% to 40%. Note that the occurrence of large supersaturations (greater than about 45%) in the simulations with waves matches the observations well. These results demonstrate the close coupling between ice concentrations and supersaturation occurrence frequencies. Without waves, ice concentrations are relatively low, and large supersaturations can persist. When numerous ice crystals nucleate in the simulations including waves, supersaturation is rapidly quenched by ice crystal growth. In other words, the deficit in occurrence of ice supersaturation in the model with waves is consistent with the excess ice concentration (Fig. 6). It should be noted here that supersaturation occurrence is probably the measurement most affected by sampling biases. The ATTREX flights generally targeted regions with cold tropopause temperatures and relatively high humidity where TTL cirrus formation was most likely. This sampling bias would tend to increase the frequency of supersaturation. In contrast, the model results represent uniform sampling along TTL trajectories. It is difficult to quantify the impact of the sampling bias on the measured ice saturation ratio frequency distribution. The discrepancies between measured and simulated occurrence of subsaturation with respect to ice (most prominent at ice saturation ratios near 0.6) probably just represent differences in the amount of dry stratospheric air included in the samples.

b. *The sensitivity of TTL cirrus to heterogeneous nuclei*

The impact of including heterogeneous nucleation on TTL cirrus microphysical properties is shown in Fig. 10. As expected, heterogeneous nucleation reduces the mean ice concentration compared to the set of simulations with homogeneous freezing only. However, even with 100 L^{-1} IN present, the cooling is occasionally rapid enough to drive homogeneous freezing events, resulting in large ice concentrations. The mean ice concentration in the set of simulations with 100 L^{-1} IN is still somewhat larger than indicated by the ATTREX FCDP and 2D-S measurements. Based on a more limited dataset of TTL cirrus microphysical properties in the eastern Pacific, Lawson et al. (2008) reported even lower mean ice concentrations (66 L^{-1}); however, the cirrus included in this study appeared to be somewhat aged with no evidence of recent ice nucleation. Using a heterogeneous nuclei population with a broad range of ice supersaturation activation thresholds and a large total IN concentration (300 L^{-1}) results in good agreement with the shape of the 2D-S ice concentration frequency distribution. Such a population of IN in the TTL could be plausible if a substantial fraction of the aerosols are glassy organics or effloresced ammonium sulfate.

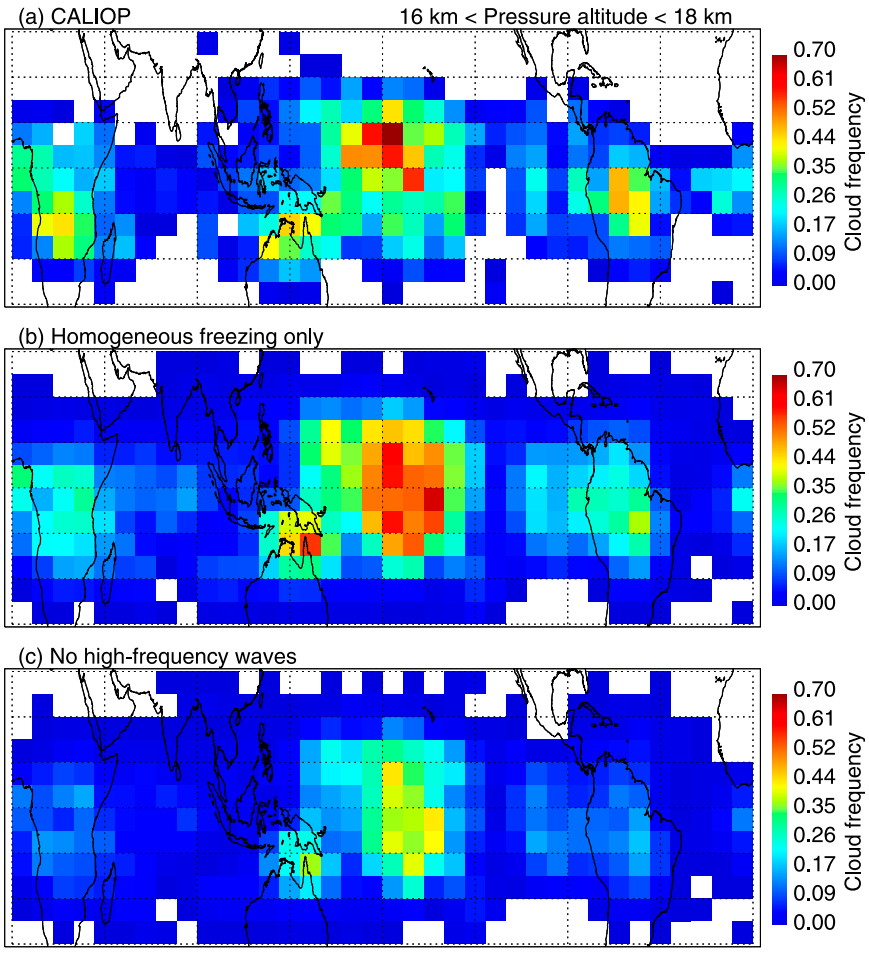

FIG. 8. Tropical distributions of upper TTL (16–18-km pressure altitude) cloud frequencies are shown. (a) CALIOP January 2007; (b) January 2007 model results with homogeneous freezing and including waves; (c) as in (b), but for results excluding high-frequency waves. Only clouds with extinctions greater than 0.005 km^{-1} are included in the model cloud frequencies.

The inclusion of heterogeneous ice nuclei appears to have a more modest impact on the statistics of TTL cirrus extinction and ice water content (Figs. 10b,c). Including 30 L^{-1} IN reduces the mean extinction from 0.069 to 0.051 km^{-1}, and increasing the IN concentration to 100 L^{-1} reduces extinction only slightly further. However, in the simulation with 300 L^{-1} IN active over a range of ice supersaturations, the mean extinction is 0.044 km^{-1}, which is considerably lower than indicated by either the ATTREX 2D-S measurements or the 2007 CALIOP measurements. Inclusion of ice nuclei changes the mean TTL cirrus ice water content by at most about 25%. Inclusion of IN slightly exacerbates the disagreement between simulated and observed TTL cirrus ice water contents. The impact of IN on the shapes of extinction and ice water content frequency distribution curves is minor.

Inclusion of heterogeneous ice nuclei has remarkably little impact on TTL cirrus occurrence frequency (Fig. 11). Likewise, the distribution of TTL cirrus is insensitive to the abundance of IN (not shown). A number of factors potentially contribute to this general lack of sensitivity. Heterogeneous nuclei allow ice nucleation at a lower ice supersaturation (30%) than homogeneous freezing ($\simeq$65%), but only about 1.2 K additional cooling is required to increase the ice saturation ratio from 1.3 to 1.65 at the tropical tropopause, and the ubiquitous waves included in these simulations typically provide the needed cooling. Heterogeneous nucleation typically produces relatively low ice concentrations such that the crystals can grow rapidly and sediment out of the supersaturated layers, resulting in short-lived clouds. Ice clouds produced by heterogeneous nucleation can, in some cases, deplete the vapor and prevent cloud formation that would have otherwise occurred downstream at a later time along the trajectories. The net result of these various effects seems to be little impact of nucleation details on TTL cirrus abundance. The water

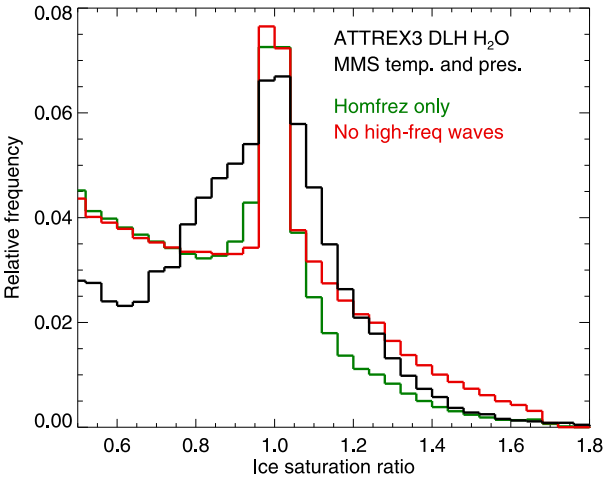

FIG. 9. Frequency distributions of TTL ice saturation ratio. The black curve is based on ATTREX DLH H_2O, MMS temperature, and MMS pressure measurements. The green curve shows results from sets of TTL cirrus simulations with homogeneous freezing only and including high-frequency waves; the red curve corresponds to a set without high-frequency waves.

vapor concentration and temperature variability dominate cloud frequency statistics in these simulations.

The inclusion of heterogeneous nucleation in TTL cirrus simulations tends to reduce the occurrence frequency of supersaturation with respect to ice (Fig. 12). Ice crystals nucleate on IN at relatively low supersaturation, and their growth limits the buildup of larger supersaturations. The result is that the comparison with ATTREX ice saturation ratio statistics degrades somewhat relative to the comparison with homogeneous freezing only. However, the differences between ice saturation ratio frequency distributions with different abundances of IN are subtle, and comparison between simulated and observed supersaturation frequency distributions likely will not be useful for assessing the impact of IN on TTL cirrus. A possible exception to this statement is the case with extremely abundant ($300\,L^{-1}$) IN active at saturation ratios ranging from 1.2 to 1.6. In this case, supersaturations larger than about 45% are essentially absent (in contrast with the observations).

As indicated in Table 1, heterogeneous nucleation is playing a significant role in production of ice in the model. For example, in the case with $100\,L^{-1}$ IN, 28% of the extinction and 50% of the ice mass comes from heterogeneously nucleated ice crystals. Nevertheless, with the possible exception of ice concentration, the statistics of TTL cirrus microphysical properties and occurrence frequency are relatively insensitive to inclusion of even a relatively high concentration of ice nuclei. This relative lack of sensitivity is primarily caused by the presence of high-frequency waves in the TTL. With the occasional strong cooling driven by waves, even relatively abundant IN do not prevent occasional homogeneous nucleation.

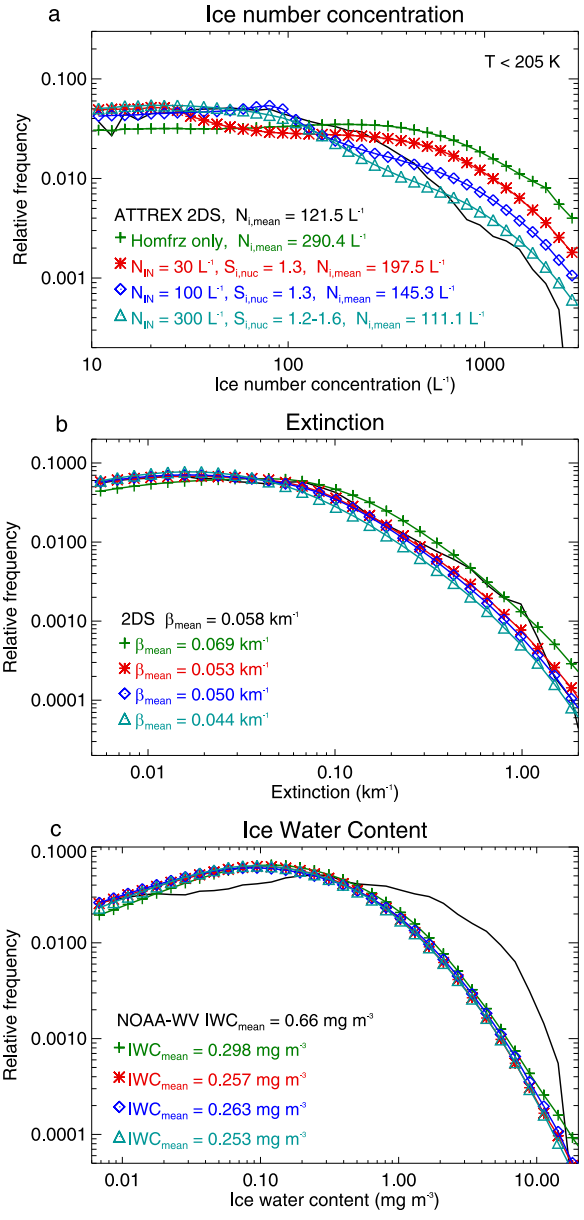

FIG. 10. As in Fig. 6, but for results showing the impact of changing IN abundance. The presence of IN does reduce the TTL-mean ice concentration somewhat; however, even with $100\,L^{-1}$ IN available, the production of large ice concentrations by rapid, wave-driven cooling is not entirely quenched. The impacts of heterogeneous nucleation on the normalized frequency distributions of extinction and ice water content are minimal.

6. Summary and discussion

We have used a combination of boreal wintertime TTL cirrus simulations and observations to statistically assess the sensitivity of TTL cirrus microphysical properties,

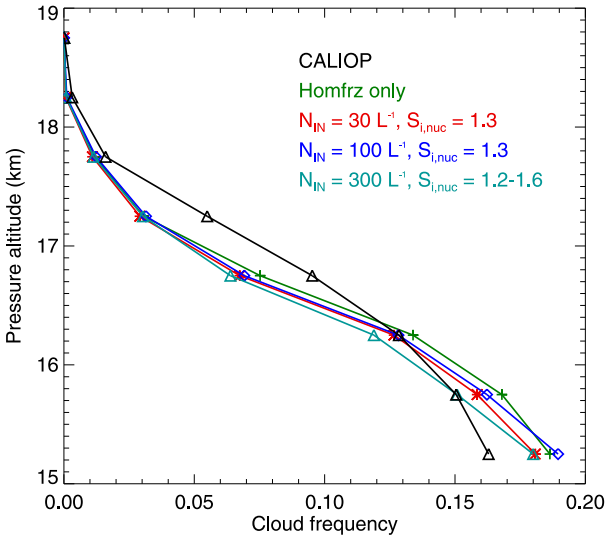

FIG. 11. As in Fig. 7, but for results showing the impact of changing IN abundance. The presence of IN does increase TTL cirrus occurrence frequency because clouds can form at lower ice supersaturations. However, the impact is minor compared to the impact of temperature variability.

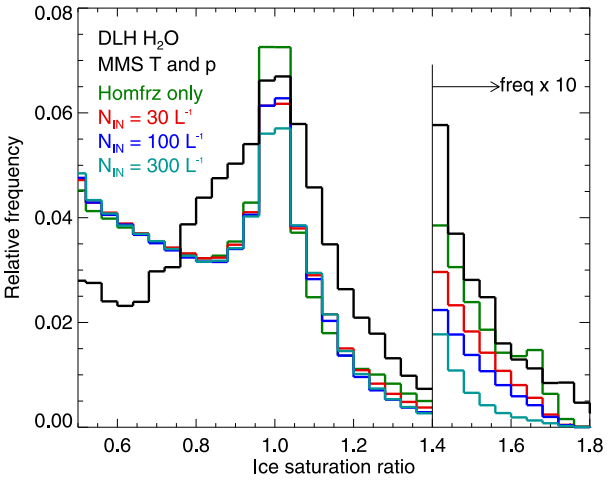

FIG. 12. As in Fig. 9, but for results showing the sensitivity to abundance of heterogeneous nuclei. Heterogeneous nucleation tends to reduce the occurrence of supersaturation with respect to ice.

cirrus occurrence frequencies, and relative humidity to TTL dynamical variability and the abundance of heterogeneous nuclei. The model includes dynamical forcing specified by ERA-Interim with small-scale waves superimposed as well as detailed treatment of cloud microphysical processes, including ice nucleation, deposition growth, sublimation, and sedimentation. The measurements and simulations lead to the following conclusions:

- The airborne in situ and satellite remote sensing measurements used in this study include more than one measurement of most of the key variables considered. Frequency distributions of ice concentrations from the ATTREX 2D-S and FCDP probes flown on the Global Hawk aircraft are in good agreement, with the exception of very large ice concentrations ($>3000\,L^{-1}$), for which the ice crystals were likely too small for detection by 2D-S (Fig. 4). The 2D-S and CALIOP TTL cirrus extinction frequency distributions agree reasonably well (certainly within the uncertainties of the measurements), although the 2D-S mean extinctions are about 20% larger than indicated by the CALIOP measurements for the same geographic region and time period. Ice water contents measured with the NOAA-H_2O instrument are about 30% larger than those determined from 2D-S measurements with the use of mass–dimensional relationships. Frequency distributions of TTL relative humidity with respect to ice constructed from the two ATTREX water vapor measurements (DLH and NOAA-H_2O) are in excellent agreement (Fig. 5).
- With homogeneous freezing of aqueous aerosols as the only ice production process, the simulated ice concentrations are considerably larger than indicated by the observations (Fig. 6). These high ice concentrations are a direct result of rapid cooling driven by the high-frequency waves that tend to be ubiquitous in the TTL; with high-frequency waves excluded, the model produces fewer ice crystals than indicated by observations. Including heterogeneous ice nuclei reduces the frequency of very high ice concentration clouds (Fig. 10). Relatively high concentrations of IN ($>300\,L^{-1}$) are required to produce good agreement with the measured frequency distribution of ice concentration.
- The extinction produced by simulations including high-frequency waves and with homogeneous freezing as the only ice nucleation process also exceed measured values (mean simulated extinctions about 16% larger than 2D-S measurements and about 33% larger than CALIOP measurements) (Fig. 6). Excluding high-frequency waves reduces the extinction by about a factor of 2 and results in simulated extinctions well below those indicated by measurements. Inclusion of heterogeneous ice nuclei in the model reduces TTL cirrus extinctions (consistent with the reduction in ice concentrations), but the extinction sensitivity is weaker than the corresponding ice concentration sensitivity (Fig. 10). However, the agreement between simulated and observed extinction is improved somewhat if heterogeneous nucleation is included.
- The model underestimates TTL cirrus ice water contents in all of the ice nucleation scenarios considered here. The IWC discrepancy between the model and observations is a factor of 2 or larger. Part of this discrepancy may be caused by sampling biases in the

ATTREX dataset (inclusion of some anvil cirrus produced by deep convection and bias toward lower TTL sampling). Ice water contents in the model are relatively insensitive to assumptions about heterogeneous nucleation (Fig. 10). Mean IWC differences are at most about 20% for the most extreme nucleation scenarios.

- The TTL cirrus occurrence frequencies in the homogeneous freezing-only simulations are in good agreement with cloud frequencies indicated by CALIOP measurements. Cloud occurrence is somewhat underestimated in the uppermost TTL and overestimated in the lower TTL (Fig. 7), and the model has too many clouds in the southern part of the western Pacific (Fig. 8). With high-frequency waves excluded, the simulated cloud frequencies are much lower than indicated by CALIOP. The simulated cloud occurrence frequencies are quite insensitive to the assumed heterogeneous nuclei abundance, either in terms of vertical distribution or geographic distribution of cloud frequency.
- The homogeneous freezing-only simulations with and without high-frequency waves bracket the observed frequency distribution of relative humidity with respect to ice (Fig. 9). This result is consistent with the differences in ice concentrations in the different simulations. The frequency of supersaturation occurrence decreases when heterogeneous nucleation is included in the model because IN nucleate ice crystals at lower supersaturations than homogeneous freezing, and increasing IN concentration exacerbates the disagreement with ATTREX relative humidity observations. In the extreme case of 300 L^{-1} IN, supersaturations greater than about 45% are essentially absent in the model, which contradicts the observed occurrences of large supersaturations. As noted above, the ATTREX flight-planning bias might have produced a dataset with more frequent ice supersaturation than would have been obtained with uniform sampling of the western Pacific TTL.

Neither the homogeneous freezing-only scenario nor any of the heterogeneous freezing specifications used here provide absolute agreement with observations of all three moments of the particle size distribution, the relative humidity, and the cloud frequency. On the other hand, given the limitations of the dataset and the measurement uncertainties, and given the lack of realistic three-dimensional dynamics or entrainment in our simulations, with the inclusion of waves and moderate numbers of heterogeneous nuclei, the simulated fields agree with the observations reasonably well. The observations of ice concentrations exceeding 1000 L^{-1} and the occurrence of supersaturations approaching the threshold for aqueous aerosol homogeneous freezing suggest that this process is responsible for TTL ice crystal production some of the time. However, some degree of heterogeneous nucleation seems to be required to avoid excessive occurrence of high ice concentrations and extinctions. Given the potential sampling biases in the limited ATTREX airborne dataset, we caution against taking the results here as compelling evidence for or against the predominance of homogeneous or heterogeneous nucleation in TTL cirrus. Perhaps the most robust result from the model–observations comparison is that some degree of high-frequency wave-driven temperature variability (beyond what is included in the global analyses) is required to explain the observed TTL cirrus cloud microphysical properties and occurrence frequencies.

The sensitivity tests presented here suggest a rather limited potential for changes in TTL cirrus as a result of changes in ice nuclei abundance. Ice crystal concentrations are significantly altered by changing IN, but cloud extinction is only moderately affected, and ice water content changes very little. Since infrared cloud radiative forcing (the dominant term in TTL cirrus net radiative forcing) scales with cloud ice water content, the net radiative forcing and local TTL radiative heating are not likely to change dramatically in response to changing TTL IN abundance. Further, since TTL cirrus frequencies appear to be insensitive to IN, the overall impact of TTL cirrus on the TTL thermal budget is not likely to be strongly dependent on IN.

We emphasize here that these results apply only to the boreal wintertime period investigated. TTL cirrus sensitivities to ice nuclei during other seasons may be very different from those indicated from this study.

Acknowledgments. This work was supported by the NASA Airborne Tropical Tropopause Experiment (ATTREX) Earth Ventures mission as well as the NASA Atmospheric Composition Campaign Data Analysis and Modeling project managed by Hal Maring and Ken Jucks.

REFERENCES

Abbatt, J. P. D., S. Benz, D. J. Cziczo, Z. Kanji, U. Lohmann, and O. Möhler, 2006: Solid ammonium sulfate aerosols as ice nuclei: A pathway for cirrus formation. *Science*, **313**, 1770–1773, doi:10.1126/science.1129726.

Anselmo, T., and Coauthors, 2007: *Cloud–Aerosol Lidar Infrared Pathfinder Satellite Observations* data management system data products catalog. NASA Langley Research Center Tech. Doc. PC-SCI-503, 100 pp.

Baker, B., and R. P. Lawson, 2006: Improvement in determination of ice water content from two-dimensional particle imagery: Part 1: Image-to-mass relationships. *J. Appl. Meteor. Climatol.*, **45**, 1282–1290, doi:10.1175/JAM2398.1.

——, Q. Mo, R. P. Lawson, A. Korolev, and D. O'Connor, 2009: Drop size distributions and the lack of small drops in RICO rain shafts. *J. Atmos. Sci.*, **48**, 616–623, doi:10.1175/2008JAMC1934.1.

Bergman, J. W., E. J. Jensen, L. Pfister, and Q. Wang, 2012: Seasonal differences of vertical-transport efficiency in the tropical

tropopause layer: On the interplay between tropical deep convection, large-scale vertical ascent, and horizontal circulations. *J. Geophys. Res.*, **117**, D05302, doi:10.1029/2011JD016992.

Comstock, J. M., T. P. Ackerman, and G. G. Mace, 2002: Ground-based lidar and radar remote sensing of tropical cirrus clouds at Nauru Island: Cloud statistics and radiative impacts. *J. Geophys. Res.*, **107**, 4714, doi:10.1029/2002JD002203.

Cziczo, D. J., and Coauthors, 2013: Clarifying the dominant sources and mechanisms of cirrus cloud formation. *Science*, **340**, 1320–1324, doi:10.1126/science.1234145.

Davis, S. M., and Coauthors, 2010: In situ and lidar observations of tropopause subvisible cirrus clouds during TC4. *J. Geophys. Res.*, **115**, D00J17, doi:10.1029/2009JD013093.

Dee, D. P., and Coauthors, 2011: The ERA-interim reanalysis: Configuration and performance of data assimilation system. *Quart. J. Roy. Meteor. Soc.*, **137**, 553–597, doi:10.1002/qj.828.

DeMott, P. J., D. C. Rogers, and S. M. Kreidenweis, 1997: The susceptibility of ice formation in upper tropospheric clouds to insoluble aerosol components. *J. Geophys. Res.*, **102**, 19 575–19 584, doi:10.1029/97JD01138.

——, D. J. Cziczo, A. J. Prenni, D. M. Murphy, S. M. Kreidenweis, D. S. Thomson, and R. Borys, 2003: Measurements of the concentration and composition of nuclei for cirrus formation. *Proc. Natl. Acad. Sci. USA*, **100**, 14 655–14 660, doi:10.1073/pnas.2532677100.

Dinh, T. P., D. R. Durran, and T. Ackerman, 2010: Maintenance of tropical tropopause layer cirrus. *J. Geophys. Res.*, **115**, D02104, doi:10.1029/2009JD012735.

——, ——, and ——, 2012: Cirrus and water vapor transport in the tropical tropopause layer—Part 1: A specific case modeling study. *Atmos. Chem. Phys.*, **12**, 9799–9815, doi:10.5194/acp-12-9799-2012.

——, S. Fueglistaler, D. R. Durran, and T. Ackerman, 2014: Cirrus and water vapor transport in the tropical tropopause layer—Part 2: Roles of ice nucleation and sedimentation, cloud dynamics, and moisture conditions. *Atmos. Chem. Phys.*, **14**, 12 225–12 236, doi:10.5194/acp-14-12225-2014.

——, A. Podglajen, A. Hertzog, B. Legras, and R. Plougonven, 2016: Effect of gravity wave temperature fluctuations on homogeneous ice nucleation in the tropical tropopause layer. *Atmos. Chem. Phys.*, **16**, 35–46, doi:10.5194/acp-16-35-2016.

Froyd, K. D., D. M. Murphy, T. J. Sanford, D. S. Thomson, J. C. Wilson, L. Pfister, and L. Lait, 2009: Aerosol composition of the tropical upper troposphere. *Atmos. Chem. Phys.*, **9**, 4363–4385, doi:10.5194/acp-9-4363-2009.

——, ——, P. Lawson, D. Baumgardner, and R. L. Herman, 2010: Aerosols that form subvisible cirrus at the tropical tropopause. *Atmos. Chem. Phys.*, **10**, 209–218, doi:10.5194/acp-10-209-2010.

Fueglistaler, S., A. E. Dessler, T. J. Dunkerton, I. Folkins, Q. Fu, and P. W. Mote, 2009: Tropical tropopause layer. *Rev. Geophys.*, **47**, RG1004, doi:10.1029/2008RG000267.

Gettelman, A., H. Morrison, S. Santos, P. Bogenschutz, and P. M. Caldwell, 2015: Advanced two-moment bulk microphysics for global models. Part II: Global model solutions and aerosol–cloud interactions. *J. Climate*, **28**, 1288–1307, doi:10.1175/JCLI-D-14-00103.1.

Haladay, T., and G. L. Stephens, 2009: Characteristics of tropical thin cirrus clouds deduced from joint *CloudSat* and *CALIPSO* measurements. *J. Geophys. Res.*, **114**, D00A25, doi:10.1029/2008JD010675.

Heymsfield, A. J., and R. M. Sabin, 1989: Cirrus crystal nucleation by homogeneous freezing of solution drops. *J. Atmos. Sci.*, **46**, 2252–2264, doi:10.1175/1520-0469(1989)046<2252:CCNBHF>2.0.CO;2.

Hoose, C., and O. Möhler, 2012: Heterogeneous ice nucleation on atmospheric aerosols: A review of results from laboratory experiments. *Atmos. Chem. Phys.*, **12**, 9817–9854, doi:10.5194/acp-12-9817-2012.

Jensen, E. J., and O. B. Toon, 1994: Ice nucleation in the upper troposphere: Sensitivity to aerosol number density, temperature, and cooling rate. *Geophys. Res. Lett.*, **21**, 2019–2022, doi:10.1029/94GL01287.

——, and ——, 1997: The potential impact of soot particles from aircraft exhaust on cirrus clouds. *Geophys. Res. Lett.*, **24**, 249–252, doi:10.1029/96GL03235.

——, and L. Pfister, 2004: Transport and freeze-drying in the tropical tropopause layer. *J. Geophys. Res.*, **109**, D02207, doi:10.1029/2003JD004022.

——, O. B. Toon, H. B. Selkirk, J. D. Spinhirne, and M. R. Schoeberl, 1996: On the formation and persistence of subvisible cirrus clouds near the tropical tropopause. *J. Geophys. Res.*, **101**, 21 361–21 375, doi:10.1029/95JD03575.

——, A. S. Ackerman, and J. A. Smith, 2007: Can overshooting convection dehydrate the tropical tropopause layer? *J. Geophys. Res.*, **112**, D11209, doi:10.1029/2006JD007943.

——, L. Pfister, T.-P. Bui, P. Lawson, and D. Baumgardner, 2010: Ice nucleation and cloud microphysical properties in tropical tropopause cirrus. *Atmos. Chem. Phys.*, **10**, 1369–1384, doi:10.5194/acp-10-1369-2010.

——, ——, and O. B. Toon, 2011: Impact of radiative heating, wind shear, temperature variability, and microphysical processes on the structure and evolution of thin cirrus in the tropical tropopause layer. *J. Geophys. Res.*, **116**, D12209, doi:1029/2010JD015417.

——, ——, and T. P. Bui, 2012: Physical processes controlling ice concentrations in cold cirrus near the tropical tropopause. *J. Geophys. Res.*, **117**, D11205, doi:10.1029/2011JD017319.

——, R. P. Lawson, J. W. Bergman, L. Pfister, T. P. Bui, and C. G. Schmitt, 2013a: Physical processes controlling ice concentrations in synoptically forced, midlatitude cirrus. *J. Geophys. Res. Atmos.*, **118**, 5348–5360, doi:10.1002/jgrd.50421.

——, and Coauthors, 2013b: Ice nucleation and dehydration in the tropical tropopause layer. *Proc. Natl. Acad. Sci. USA*, **110**, 2041–2046, doi:10.1073/pnas.1217104110.

——, and Coauthors, 2016: The NASA Airborne Tropical Tropopause Experiment (ATTREX): High-altitude aircraft measurements in the tropical western Pacific. *Bull. Amer. Meteor. Soc.*, doi:10.1175/BAMS-D-14-00263.1, in press.

Kärcher, B., 2004: Cirrus clouds in the tropical tropopause layer: Role of heterogeneous ice nuclei. *Geophys. Res. Lett.*, **31**, L12101, doi:10.1029/2004GL019774.

——, and U. Lohmann, 2002: A parameterization of cirrus cloud formation: Homogeneous freezing of supercooled aerosols. *J. Geophys. Res.*, **107**, AAC 4-1–AAC 4-10, doi:10.1029/2001JD000470.

——, and J. Ström, 2003: The roles of dynamical variability and aerosols in cirrus cloud formation. *Atmos. Chem. Phys.*, **3**, 823–838, doi:10.5194/acp-3-823-2003.

——, J. Hendricks, and U. Lohmann, 2006: Physically based parameterization of cirrus cloud formation for use in global atmospheric models. *J. Geophys. Res.*, **111**, D01205, doi:10.1029/2005JD006219.

Kim, J.-E., and M. J. Alexander, 2013: A new wave scheme for trajectory simulations of stratospheric water vapor. *Geophys. Res. Lett.*, **40**, 5286–5290, doi:10.1002/grl.50963.

Koop, T., B. Luo, A. Tsias, and T. Peter, 2000: Water activity as the determinant for homogeneous ice nucleation in aqueous solutions. *Nature*, **406**, 611–614, doi:10.1038/35020537.

Krämer, M., and Coauthors, 2009: Ice supersaturations and cirrus cloud crystal numbers. *Atmos. Chem. Phys.*, **9**, 3505–3522, doi:10.5194/acp-9-3505-2009.

Lawson, R. P., 2011: Effects of ice particles shattering on the 2D-S probe. *Atmos. Meas. Tech.*, **4**, 1361–1381, doi:10.5194/amt-4-1361-2011.

——, B. A. Baker, C. G. Schmitt, and T. L. Jensen, 2001: An overview of microphysical properties of Arctic clouds observed in May and July during FIRE ACE. *J. Geophys. Res.*, **106**, 14 989–15 014, doi:10.1029/2000JD900789.

——, ——, B. Pilson, and Q. Mo, 2006a: In situ observations of the microphysical properties of wave, cirrus, and anvil clouds. Part II: Cirrus clouds. *J. Atmos. Sci.*, **63**, 3186–3203, doi:10.1175/JAS3803.1.

——, D. O'Connor, P. Zmarzly, K. Weaver, B. A. Baker, Q. Mo, and H. Jonsson, 2006b: The 2D-S (stereo) probe: Design and preliminary tests of a new airborne, high-speed, high-resolution imaging probe. *J. Atmos. Oceanic Technol.*, **23**, 1462–1477, doi:10.1175/JTECH1927.1.

——, B. Pilson, B. A. Baker, Q. Mo, E. J. Jensen, L. Pfister, and P. Bui, 2008: Aircraft measurements of microphysical properties of subvisible cirrus clouds in the tropical tropopause layer. *Atmos. Chem. Phys.*, **8**, 1609–1620, doi:10.5194/acp-8-1609-2008.

Lohmann, U., B. Kärcher, and J. Hendricks, 2004: Sensitivity studies of cirrus clouds formed by heterogeneous freezing in the ECHAM GCM. *J. Geophys. Res.*, **109**, D16204, doi:10.1029/2003JD004443.

Massie, S., A. Gettelman, and W. Randel, 2002: The distribution of tropical cirrus in relation to convection. *J. Geophys. Res.*, **107**, 4591, doi:10.1029/2001JD001293.

McFarquhar, G. M., J. Um, M. Freer, D. Baumgardner, G. L. Kok, and G. Mace, 2007: The importance of small ice crystals to cirrus properties: Observations from the Tropical Warm Pool International Cloud Experiment (TWP-ICE). *Geophys. Res. Lett.*, **57**, L13803, doi:10.1029/2007GL029865.

Möhler, O., and Coauthors, 2003: Experimental investigation of homogeneous freezing of sulphuric acid particles in the aerosol chamber AIDA. *Atmos. Chem. Phys.*, **3**, 211–223, doi:10.5194/acp-3-211-2003.

Murphy, D. M., 2014: Rare temperature histories and cirrus ice number density in a parcel and one-dimensional model. *Atmos. Chem. Phys.*, **14**, 13 013–13 022, doi:10.5194/acp-14-13013-2014.

Murray, B. J., 2008: Inhibition of ice crystallisation in highly viscous aqueous organic acid droplets. *Atmos. Chem. Phys.*, **8**, 5423–5433, doi:10.5194/acp-8-5423-2008.

——, and Coauthors, 2010: Heterogeneous nucleation of ice particles on glassy aerosols under cirrus conditions. *Nat. Geosci.*, **3**, 233–237, doi:10.1038/ngeo817.

Oltmans, S. J., and K. H. Rosenlof, 2000: Data quality. SPARC assessment of upper tropospheric and stratospheric water vapour. SPARC Tech. Rep. 2, 95–194.

Pfister, L., and Coauthors, 2001: Aircraft observations of thin cirrus clouds near the tropical tropopause. *J. Geophys. Res.*, **106**, 9765–9786, doi:10.1029/2000JD900648.

Pruppacher, H. R., and J. D. Klett, 1997: *Microphysics of Clouds and Precipitation*. Kluwer Academic Publishers, 954 pp.

Read, W. G., and Coauthors, 2007: Aura Microwave Limb Sounder upper tropospheric and lower stratospheric H_2O and relative humidity with respect to ice validation. *J. Geophys. Res.*, **112**, D24S35, doi:10.1029/2007JD008752.

Riihimaki, L. D., and S. A. McFarlane, 2010: Frequency and morphology of tropical tropopause layer cirrus from *CALIPSO* observations: Are isolated cirrus different from those connected to deep convection? *J. Geophys. Res.*, **115**, D18201, doi:10.1029/2009JD013133.

——, ——, C. Liang, S. T. Massie, N. Beagley, and T. D. Toth, 2012: Comparison of methods to determine tropical tropopause layer cirrus formation mechanisms. *J. Geophys. Res.*, **117**, D06218, doi:10.1029/2011JD016832.

Sassen, K., and G. C. Dodd, 1989: Haze particle nucleation simulations in cirrus clouds, and applications for numerical and lidar studies. *J. Atmos. Sci.*, **46**, 3005–3014, doi:10.1175/1520-0469(1989)046<3005:HPNSIC>2.0.CO;2.

Spichtinger, P., and D. J. Cziczo, 2010: Impact of heterogeneous ice nuclei on homogeneous freezing events in cirrus clouds. *J. Geophys. Res.*, **115**, D14208, doi:10.1029/2009JD012168.

——, and M. Krämer, 2013: Tropical tropopause ice clouds: A dynamic approach to the mystery of low crystal numbers. *Atmos. Chem. Phys.*, **13**, 9801–9818, doi:10.5194/acp-13-9801-2013.

Thornberry, T. D., A. W. Rollins, R. S. Gao, L. A. Watts, S. J. Ciciora, R. J. McLaughlin, and D. W. Fahey, 2015: A two-channel, tunable diode laser-based hygrometer for measurement of water vapor and cirrus cloud ice water content in the upper troposphere and lower stratosphere. *Atmos. Meas. Tech.*, **8**, 211–244, doi:10.5194/amt-8-211-2015.

Ueyama, R., L. Pfister, E. J. Jensen, G. S. Diskin, T. P. Bui, and J. M. Dean-Day, 2014: Dehydration in the tropical tropopause layer: A case study for model evaluation using aircraft observations. *J. Geophys. Res. Atmos.*, **119**, 5299–5316, doi:10.1002/2013JD021381.

——, E. J. Jensen, L. Pfister, and J.-E. Kim, 2015: Dynamical, convective, and microphysical control on wintertime distributions of water vapor and clouds in the tropical tropopause layer. *J. Geophys. Res. Atmos.*, **120**, 10 483–10 500, doi:10.1002/2015JD023318.

Wang, P.-H., P. Minnis, M. P. McCormick, G. S. Kent, and K. M. Skeens, 1996: A 6-year climatology of cloud occurrence frequency from Stratospheric Aerosol and Gas Experiment II observations (1985–1990). *J. Geophys. Res.*, **101**, 29 407–29 429, doi:10.1029/96JD01780.

Weinstock, E. M., and Coauthors, 2009: Validation of the Harvard Lyman-α in situ water vapor instrument: Implications for the mechanisms that control stratospheric water vapor. *J. Geophys. Res.*, **114**, D23301, doi:10.1029/2009JD012427.

Whiteway, J., and Coauthors, 2004: Anatomy of cirrus clouds: Results from the Emerald airborne campaign. *Geophys. Res. Lett.*, **31**, L24102, doi:10.1029/2004GL021201.

Wilson, T. W., and Coauthors, 2012: Glassy aerosols with a range of compositions nucleate ice heterogeneously at cirrus temperatures. *Atmos. Chem. Phys.*, **12**, 8611–8632, doi:10.5194/acp-12-8611-2012.

Wright, J. S., and S. Fueglistaler, 2013: Large differences in reanalyses of diabatic heating in the tropical upper troposphere and lower stratosphere. *Atmos. Chem. Phys.*, **13**, 9565–9576, doi:10.5194/acp-13-9565-2013.

Yang, Q., Q. Fu, and Y. Hu, 2010: Radiative impacts of clouds in the tropical tropopause layer. *J. Geophys. Res.*, **115**, D00H12, doi:10.1029/2009JD012393.

Young, S. A., and M. A. Vaughan, 2009: The retrieval of profiles of particulate extinction from *Cloud–Aerosol Lidar Infrared Pathfinder Satellite Observations* (*CALIPSO*) data: Algorithm description. *J. Atmos. Oceanic Technol.*, **26**, 1105–1119, doi:10.1175/2008JTECHA1221.1.

Zobrist, B., C. Marcolli, D. A. Pedernera, and T. Koop, 2008: Do atmospheric aerosols form glasses? *Atmos. Chem. Phys.*, **8**, 5221–5244, doi:10.5194/acp-8-5221-2008.